INTERNATIONAL JOURNAL OF CLIMATOLOGY
Int. J. Climatol. (2015)
Published online in Wiley Online Library
(wileyonlinelibrary.com) DOI: 10.1002/joc.4352

RMetS
Royal Meteorological Society

Trend and interannual variation in summer precipitation in eastern Siberia in recent decades

Hatsuki Fujinami,[a]* Tetsuzo Yasunari[b] and Tatsuro Watanabe[c]

[a] *Hydrospheric Atmospheric Research Center, Nagoya University, Japan*
[b] *Research Institute for Humanity and Nature, Kyoto, Japan*
[c] *Graduate School of Environmental Sciences, Nagoya University, Japan*

ABSTRACT: We analysed the long-term trend and interannual variability in summer (JJA) precipitation over eastern Siberia (90°–140°E, 50°–70°N) for the period 1979–2007. An increasing trend in summer precipitation was observed over large areas (Yenisei and Lena river basins) of eastern Siberia. Summer mean 850-hPa geopotential height decreased from Siberia to the marginal seas north of Siberia, with the largest decreases occurring over the northern part of eastern Siberia, while increasing trends were found around Mongolia, inducing a significant increase in westerly moisture flux and its convergence over eastern Siberia. Empirical orthogonal function (EOF) analysis of detrended summer precipitation revealed the leading modes of the interannual variability. The first leading mode (EOF1) represents interannual variation around the central Siberian Plateau and the middle reaches of the Lena river basin, related to the enhancement of a low-level cyclonic circulation centred on 65°N, 100°E around eastern Siberia. The circulation pattern of EOF1 closely matches the trend pattern over Siberia, indicating that a deeper quasi-stationary trough appears with increasing frequency in recent decades. The second leading mode (EOF2) shows a dipole pattern between the middle reaches of the Lena river basin and the western part of the Central Siberian Plateau. Wet summers in the Lena river basin are related to a stationary trough centred at around 60°N, 130°E. These leading patterns are related to the change in position of the stationary trough and the ridge of the wave train structure along the Arctic polar jet across the northern Eurasian continent.

KEY WORDS Eastern Siberia; summer precipitation; hydroclimate; trend; interannual variation; stationary trough; polar jet

Received 1 August 2014; Revised 25 February 2015; Accepted 27 March 2015

1. Introduction

Eastern Siberia possesses a vast region of coniferous forest known as taiga. The forest is maintained under very dry conditions with a total annual precipitation of ~200–300 mm (Fukutomi *et al.*, 2003; Ohta *et al.*, 2008). In eastern Siberia, the larch-dominated taiga has a spatially homogeneous distribution over the continuous and discontinuous permafrost. In summer, the surface layer (i.e. the active layer) of permafrost thaws and provides liquid water to tree roots. The boundary between the surface active layer and permafrost acts as an impermeable layer, and a small amount of rainfall and meltwater is retained in the surface layer, without infiltration into deeper layers. Thus, the existence of permafrost allows a vast area of forest to be maintained under dry conditions, forming a unique taiga–permafrost coupled system in eastern Siberia (Osawa *et al.*, 2010; Zhang *et al.*, 2011).

The taiga plays an important role in the hydroclimate of eastern Siberia (Ohta *et al.*, 2001; Saito *et al.*, 2006; Ohta *et al.*, 2008). Ohta *et al.* (2001) reported from *in situ* observations that the total evapotranspiration from the forest (151 mm) exceeded the precipitation (106 mm) and was equal to 73% of the total water input (211 mm), including snow-melt water during the forest growing season (mid-April to early September) in 1998. Precipitation reaches a maximum (minimum) in July (February) in the seasonal cycle (Fukutomi *et al.*, 2003; Serreze and Etringer, 2003). Summer precipitation (June–August; JJA) accounts for more than 40% of the total annual precipitation, indicating its importance to the hydroclimate in eastern Siberia. Atmospheric water budget analysis can estimate the contribution of evaporation/evapotranspiration and large-scale moisture flux divergence to precipitation (e.g. Fukutomi *et al.*, 2003; Serreze and Etringer, 2003; Yatagai, 2003). If we assume that the tendency of precipitable water in the atmosphere is negligible, the water budget equation can be simplified to state that precipitation equals the sum of evaporation/evapotranspiration and moisture flux convergence: $\langle P \rangle = \langle E \rangle - \langle \nabla \cdot Q \rangle$, where P is precipitation, E is evaporation/evapotranspiration, $\langle \nabla \cdot Q \rangle$ is the divergence of vertically integrated moisture flux, and angled brackets denote the area average. According to the atmospheric water budget, summer precipitation over east Siberia originates predominantly from evaporation/evapotranspiration from the land surface, whereas the contribution of the large-scale moisture flux convergence is small (Fukutomi

* Correspondence to: Dr H. Fujinami, Hydrospheric Atmospheric Research Center, Nagoya University, Furo-cho, Chikusa-ku, Nagoya 464-8601, Japan. E-mail: hatsuki@hyarc.nagoya-u.ac.jp

et al., 2003; Serreze and Etringer, 2003; Serreze *et al.*, 2003). Thus, summer precipitation is controlled mainly by the contribution of recycled water from the land surface (Kurita *et al.*, 2004).

In contrast, on interannual timescales, the variation of the large-scale moisture convergence becomes the main driver of summer precipitation variability over eastern Siberia (Fukutomi *et al.*, 2003) because the interannual variation of evaporation/evapotranspiration is small compared with the large fluctuations in precipitation in eastern Siberia during summer (Fukutomi *et al.*, 2003; Ohta *et al.*, 2008). The taiga–permafrost coupling maintains a constant amount of evapotranspiration (Sugimoto *et al.*, 2002; Ohta *et al.*, 2008). These observations suggest that knowledge of the variability of large-scale summer precipitation is essential in understanding the hydroclimate of the region.

Fukutomi *et al.* (2003) reported that the dominant mode of interannual variation in the large-scale precipitation anomaly over Siberia is an east–west seesaw oscillation between eastern and western Siberia, with a timescale of ∼6–8 years. Cyclone tracks are closely clustered in relation to the seesaw oscillation: cyclones frequently pass over eastern (western) Siberia in wet years in eastern (western) Siberia, while a significant decrease in cyclone tracks is observed in western (eastern) Siberia. Thus, the east–west seesaw oscillation is strongly related to the east–west shift of storm tracks across Siberia (Fukutomi *et al.*, 2004, 2007). Iwao and Takahashi (2006) showed that the dominant mode of the interannual fluctuation in July precipitation is a north–south seesaw pattern between northeast Asia and Siberia.

However, these previous studies did not focus on the variation in summer precipitation over eastern Siberia, where the larch taiga–climate interaction through the water cycle is dominant. Few studies have investigated the variability of summer precipitation in eastern Siberia, or the precipitation trend in recent decades. Therefore, this study examines the spatial patterns in the trend and interannual variation of summer precipitation in eastern Siberia, and the associated atmospheric circulation fields. The remainder of the manuscript is organized as follows. Section 2 introduces datasets and methods. The results, in terms of precipitation trends, the leading modes of interannual precipitation variability in eastern Siberia, and their associated atmospheric circulation patterns, are given in Section 3. Section 4 discusses the long-term trend and the recent change in hydroclimate over eastern Siberia. Finally, the conclusions are presented in Section 5.

2. Data and methods

The analysis of precipitation variability was based on the APHRODITE V1101 dataset for northern Eurasia (hereafter, APHRODITE-RU) (Yatagai *et al.*, 2012). APHRODITE-RU consists of daily gridded precipitation datasets, derived from quality-controlled rain gauge data. The number of valid rain gauge stations is much greater than that available from the Global Telecommunication System (GTS). The daily precipitation data enable the analysis of precipitation characteristics, such as the frequency and intensity, on a daily basis. Thus, APHRODITE-RU has an advantage over other long-term precipitation datasets that provide data on a monthly basis. The precipitation frequency was defined as the total number of days with more than 1.0 mm day^{-1} of precipitation during the summer (JJA). Daily precipitation intensity was expressed as the total summer rainfall divided by the frequency. The dataset is on a 0.5° latitude–longitude grid. We also used the Japanese 25-year (1979–2004) reanalysis (JRA25)/Japan Meteorological Agency (JMA) Climate Data Assimilation system (JCDAS) datasets on a 1.25° latitude–longitude grid to examine large-scale atmospheric circulation associated with rainfall variability (Onogi *et al.*, 2007). The JRA25/JCDAS dataset covers the period 1979–2013. The dataset variables include horizontal wind (u and v), specific humidity (q), and geopotential height (Z). The vertically integrated water vapour flux from the surface to 100 hPa was also calculated. The data were monthly averaged from the original 6 hourly data. We used both datasets from 1979 to 2007 (29 years), during the summer season (JJA). Monthly global Normalised Difference Vegetation Index (NDVI) data obtained from the Pathfinder advanced very high resolution radiometer (AVHRR) Land (PAL) dataset, with 1° × 1° resolution, were also used to show the spatial distribution of vegetation over eastern Siberia for the period 1980–2000 (Smith *et al.*, 1997; Suzuki *et al.*, 2007).

To investigate the variability of precipitation in eastern Siberia, we define a rectangular domain of 50°–70°N, 90°–140°E (Figure 1), characterised by higher elevation than the West Siberian Plain to the west of 90°E. The Central Siberian Plateau extends over the northwestern part of the domain, and high mountain ranges are present in its southern and eastern parts. The Lena river basin is located between these ranges. The domain also contains parts of the Yenisei river and Amur river basins in its western and southeastern-most areas, respectively.

First, we calculated the long-term trend of JJA-total precipitation over eastern Siberia during 1979–2007. The non-parametric Mann–Kendall test was applied to assess the trend. Then, we used empirical orthogonal function (EOF) analysis to examine the leading modes of interannual variability in JJA precipitation over eastern Siberia. The linear trend was removed from the original time series at each grid point before applying EOF analysis. The total precipitation in summer varies from less than 100 mm in the northern part of the analysis domain to more than 300 mm in the southeastern part (Figure 2(a)). Therefore, to detect the spatial pattern of the leading mode, which includes an area of relatively low precipitation, EOF analysis was applied to normalised and detrended JJA precipitation data from 1979 to 2007 in the domain, providing similar results to EOF analysis using a correlation matrix (Wilks, 2011). The spatial structure of each EOF represents the spatial distribution of the correlation coefficient between the precipitation value at each grid point and

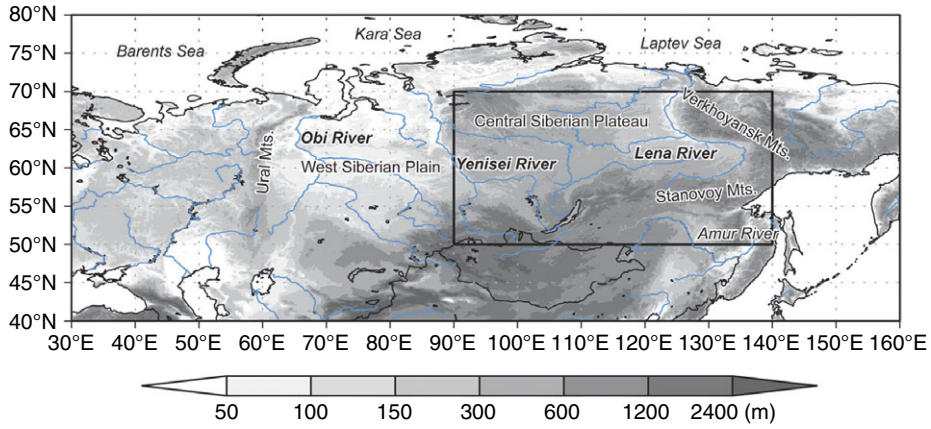

Figure 1. Shaded relief map of Siberia. The domain enclosed by the rectangle is the key domain used to examine precipitation variability in this study and is referred to as eastern Siberia.

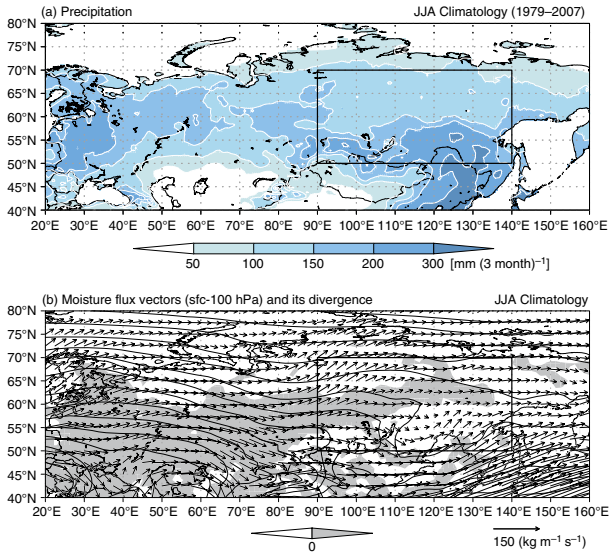

Figure 2. (a) Climatological (1979–2007) mean distribution of summer (JJA) total precipitation. (b) As in (a), but for vertically integrated (from the surface to 100 hPa) moisture flux vectors and divergence. Shading denotes areas of divergent moisture flux.

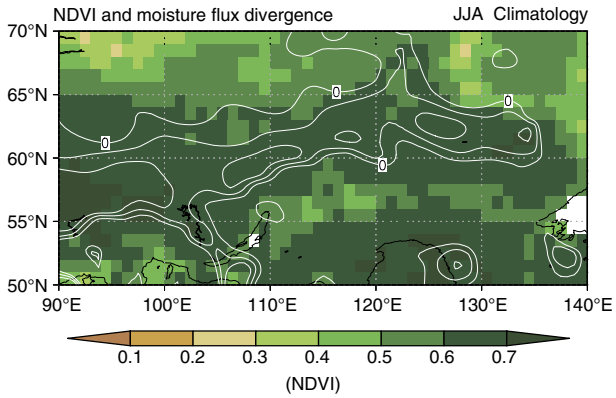

Figure 3. Climatological (1980–2000) seasonal (JJA) mean distribution of NDVI over eastern Siberia (shading) and moisture flux divergence (1.0×10^{-6} kg m^{-2} s^{-1}; contours). Contours are drawn only in areas of divergent moisture flux, at 0, 5, and 10×10^{-6} kg m^{-2} s^{-1}.

the principal component (PC), because the PCs are normalised. Before EOF analysis, we multiplied the data by a weighting factor: the square root of the cosine of latitude. The statistical significance of the composite and regression fields at each grid point was estimated using Student's *t*-test.

3. Results

3.1. Climatological features

Climatological mean summer total precipitation displays a zonal distribution over Siberia (Figure 2(a)). Precipitation is less than 200 mm, except over the southern part of the domain. In eastern Siberia, the precipitation distribution is characterised by a large meridional gradient from south to north, partly due to the existence of mountains located around the southeastern part of the analysis domain (Yoshida *et al.*, 2011). Westerly moisture flux vectors predominate over Siberia, and the area of moisture flux divergence extends zonally along 60°N. This means that evaporation/evapotranspiration from the surface is a major source of summer precipitation over the area, which is in agreement with the results of an atmospheric water budget analysis for the Lena, Obi, and Yenisei river basins by Fukutomi *et al.* (2003) and Serreze and Etringer (2003). Note that the dense vegetation area, as determined by NDVI, corresponds well to the area of moisture flux divergence in JJA (Figure 3), suggesting that boreal forest (i.e. taiga) is an important source of moisture through evapotranspiration during summer.

3.2. Trend in summer precipitation over eastern Siberia

A significant trend in summer precipitation is observed over eastern Siberia (Figure 4). An increasing trend is found over most of eastern Siberia (e.g. the Yenisei river basin and Lena river basin) except in the southeastern part of the domain where there is a decreasing trend. The time series of area-averaged JJA total precipitation for 55°–70°N, 90°–130°E from APHRODITE-RU shows a remarkable increasing trend over eastern Siberia with

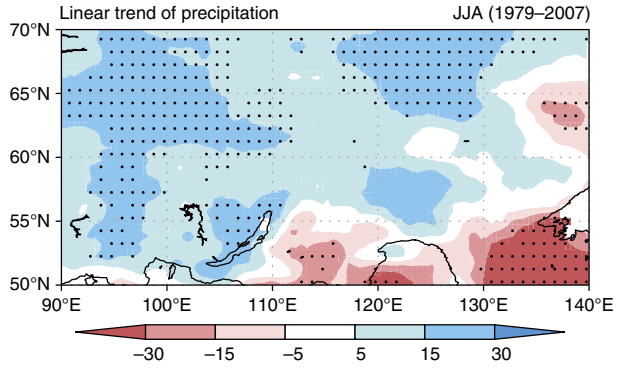

Figure 4. Linear trend (per decade) of summer total precipitation [mm (3 months)$^{-1}$] over eastern Siberia for 1979–2007. Solid dots denote grid points with trends that are statistically significant at the 95% confidence level.

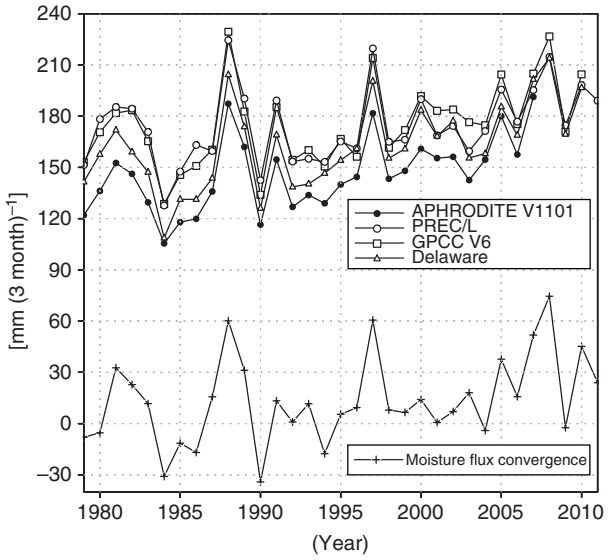

Figure 5. Time series of area-averaged (55°–70°N, 90°–130°E) 3-month (JJA) total precipitation in eastern Siberia from four different datasets (APHRODITE, GPCC, PREC/L, and Delaware). The time series of moisture flux convergence from JRA25 is also shown. The unit of moisture flux convergence (kg m^{-2} s^{-1}) is converted into mm (3 month)$^{-1}$ for the comparison with the JJA total precipitation.

interannual fluctuation on a 3–5-year period (Figure 5). There is a linear trend in the time series with a 13.9-mm increase per decade during 1979–2007, which is significant at the 99% level (Mann–Kendall test).

The increasing trend can also be observed until recently in other monthly precipitation datasets such as the Global Precipitation Climatology Centre (GPCC) (Schneider *et al.*, 2014), Precipitation Reconstruction over Land (PREC/L) (Chen *et al.*, 2002), and the University of Delaware precipitation (Willmott and Matsuura, 1995), with 0.5°×0.5° latitude–longitude grids (Figure 5). The time series of these four datasets show a similar increasing trend and interannual variation from 1979 to 2007, although the precipitation in APHRODITE is the lowest of all the datasets. Yatagai *et al.* (2012) reported that APHRODITE data underestimated precipitation

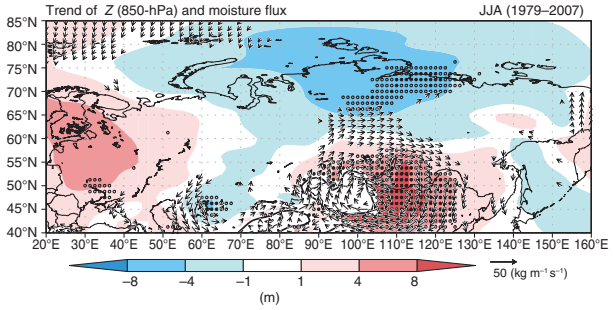

Figure 6. Linear trend (per decade) of 850-hPa geopotential height (Z) and vertically integrated moisture flux vectors for 1979–2007. Solid (open) dots denote grid points with trends in geopotential height that are statistically significant at the 95% (90%) confidence level. Moisture flux vectors are plotted where either the u or v component exceeds the 95% confidence level.

compared with monthly precipitation datasets. As in APHRODITE-RU, the increasing trends observed in GPCC and the Delaware dataset from 1979 to 2010 are statistically significant at the 99% level. The increasing trend in PREC/L from 1979 to 2011 is statistically significant at the 95% level. Thus, the increasing trend is a robust feature of precipitation over eastern Siberia, although the absolute values of precipitation and their linear trends differ slightly between datasets.

Figure 6 shows the linear trend of summer mean 850-hPa geopotential height (Z850) and vertically integrated moisture flux vectors. Summer mean Z850 decreases from Siberia to the marginal seas north of Siberia, with the largest decreases occurring over the northern part of eastern Siberia. The spatial structure of the trend in Z850 around Siberia is consistent with that in surface pressure during the period 1979–2007 shown by Ogi and Wallace (2007, their Figure 4(c)). In contrast, Z850 around Mongolia shows a significant increase. The spatially varying feature of trends in geopotential height over and around Siberia suggests that atmospheric circulation changes contribute to the increasing trend in precipitation over eastern Siberia. The structure of the trend in Z850 induces a significant strengthening in westerly moisture flux over eastern Siberia. The area of increasing precipitation trend over eastern Siberia is consistent with the area where the decreasing Z850 trend and the increasing trend of westerly moisture flux are observed. An increasing trend in the moisture flux convergence is also found over eastern Siberia (Figure 5), consistent with the increasing trend in precipitation, and this is statistically significant at the 90% level for the period 1979–2011. This means that moisture flux convergence is likely to be a key factor causing the trend of precipitation over eastern Siberia.

3.3. Leading modes of interannual variability in summer precipitation over eastern Siberia

The three leading EOFs and PCs of summer precipitation are shown in Figure 7. The first three EOFs account for 49.6% of the total variance, with the first EOF explaining 20.2%. Positive values of EOF1 are spread widely over the

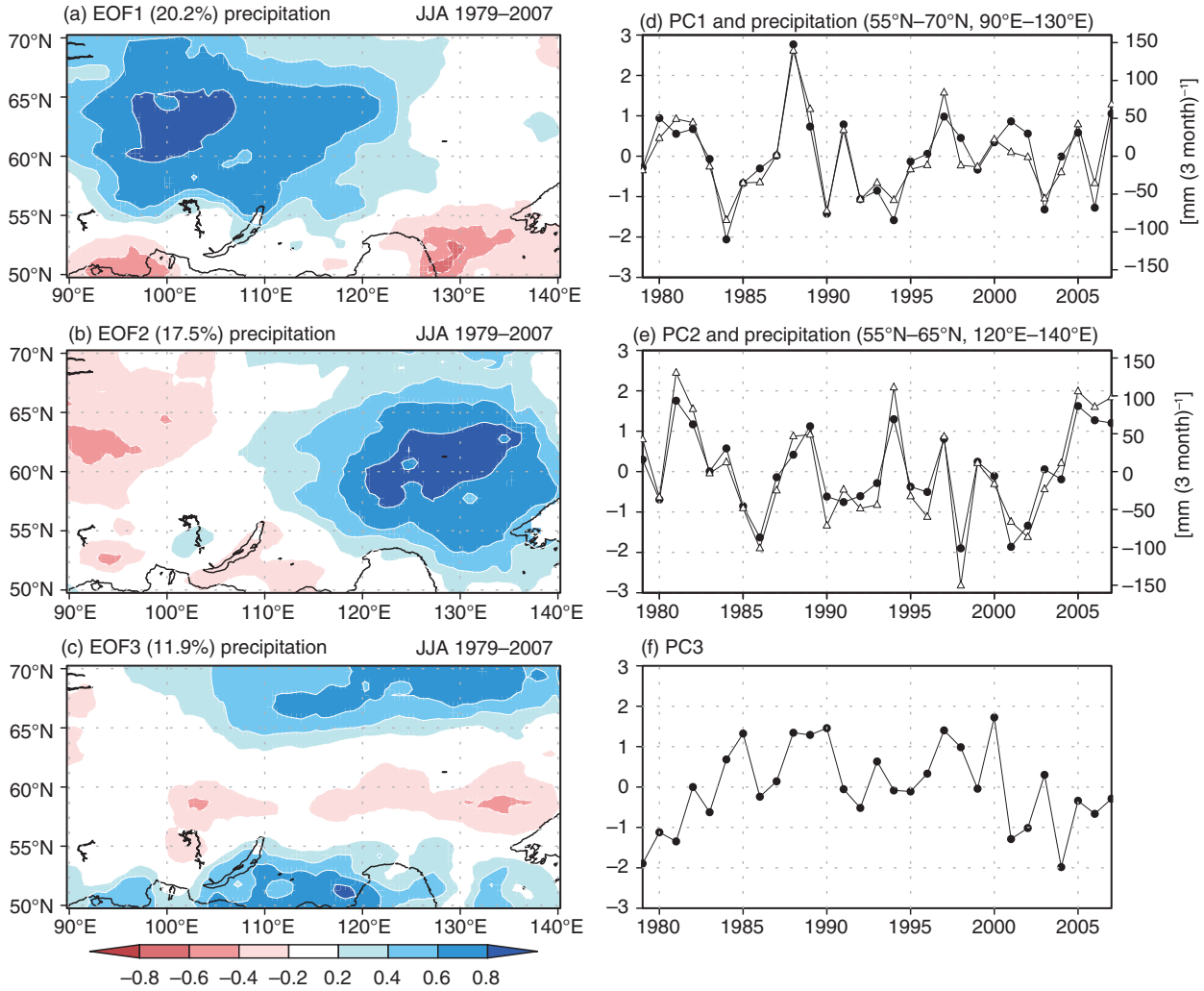

Figure 7. Spatial patterns of the first three leading EOF modes of summer precipitation over eastern Siberia: (a) EOF1, (b) EOF2, and (c) EOF3, and time series of the first three PCs (solid line with solid circles): (d) PC1, (e) PC2, and (f) PC3. The solid line with open triangles in (d) indicates the area-averaged precipitation for 55°–70°N, 90°–130°E, and in (e) for 55°–65°N, 120°–140°E.

Central Siberian Plateau, including the middle reaches of the Yenisei river basin, and the upper to lower reaches of the Lena river basin, while negative values occur around the lower reaches of the Amur river basin. The spatial pattern of EOF1 is similar to that of the precipitation trend shown in Figure 4. The time series of PC1 reveals interannual fluctuations with a 3–5-year period (Figure 7(d)). The time variation of the detrended rainfall averaged over the area where positive values exist in Figure 7(a) (55°–70°N, 90°–130°E) is almost identical to PC1 (Figure 7(d)).

EOF2 represents a dipole pattern between the middle reaches of the Lena river basin with a positive centre around 60°N, 130°E and a negative area around the westernmost part of the analysis domain. This mode explains 17.5% of the total variance. PC2 displays interannual variability with a timescale of ∼6–8 years (Figure 7(e)). The spatiotemporal structure from EOF2 and PC2 resembles the precipitation seesaw pattern between the Lena and Obi river basins at a timescale of ∼6–8 years as reported by Fukutomi *et al.* (2003) and Fukutomi *et al.* (2007). The correlation between PC2 and the precipitation seesaw index (defined by Fukutomi *et al.* 2007) is 0.75, which is significant at the 99% level. A time series of area-averaged precipitation anomaly around the positive area of EOF2 (i.e. 55°–65°N, 120°–140°E) corresponds closely to PC2, which displays large positive values from 2005 to 2007. In EOF3 (Figure 7(c)), the positive areas extend over the mountainous regions of the northeast (around the Verkhoyansk Mountains) and the southern parts of eastern Siberia (around the boundary with Mongolia). However, these values are small compared with those seen in EOF1 and EOF2. Values are negative along 60°N, between the positive areas, but the values are very small. Positive values generally continued from the mid-1980s to 2000, while negative values occurred in other years (Figure 7(f)).

3.4. Distribution of precipitation and large-scale atmospheric circulation related to the leading modes

Figure 8 shows the regression patterns in Z850 and the vertically integrated moisture flux vectors based on the first three PCs. Note that the figures cover a broader area than the domain used for the EOF analysis. In EOF1,

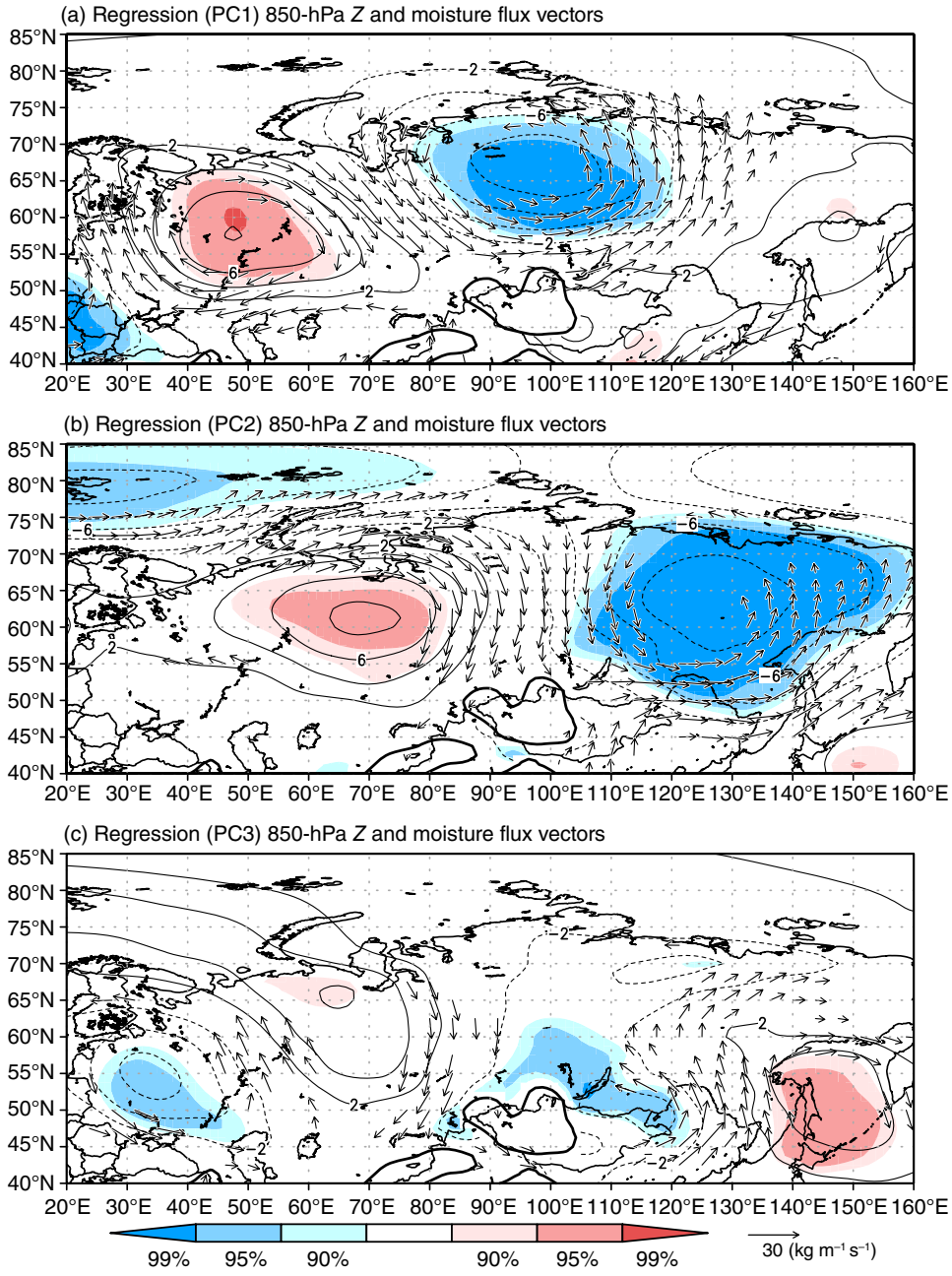

Figure 8. Regression patterns of the 850-hPa geopotential height (contours, interval 2 gpm), and vertically integrated moisture flux vectors based on (a) PC1, (b) PC2, and (c) PC3. The colour shading represents the confidence level of the correlation coefficient between each PC and the 850-hPa geopotential height. Blue (red) shading indicates negative (positive) correlation. Only moisture flux vectors statistically significant at the 95% level are plotted. The topographic contour for 1500 m is shown as a thick solid line.

a cyclonic circulation anomaly centred at around 65°N, 100°E (Figure 8(a)) is associated with wet summers. The cyclonic circulation anomaly extends over a broad area from eastern Siberia to the marginal seas to the north (i.e. the Laptev and Kara seas). It enhances westerly moisture flux anomalies along latitudes from 50° to 65°N toward eastern Siberia. South and southwesterly moisture flux vectors also dominate over the eastern part of eastern Siberia. Note that the regression pattern in EOF1 is similar to the trend pattern of Z850 shown in Figure 6 except around Mongolia, indicating a physical linkage between the trend and the interannual variability in Z850 related to EOF1. The regression pattern for EOF2 has a dipole pattern between the Obi and Lena river basins (Figure 8(b)). High summer precipitation around the middle reaches of the Lena river basin is related to the cyclonic circulation anomaly centred around 65°N, 130°E. The structure of the anomaly is similar to that of the seesaw mode between the two river basins as reported by Fukutomi *et al.* (2003). Circulation anomalies in EOF3 do not exhibit large signals over eastern Siberia (Figure 8(c)). Weak and relatively local cyclonic anomalies are located around the positive values seen in EOF3 (Figure 7(c)). Herein, we focus on the atmospheric structure in relation to EOF1 and 2, because

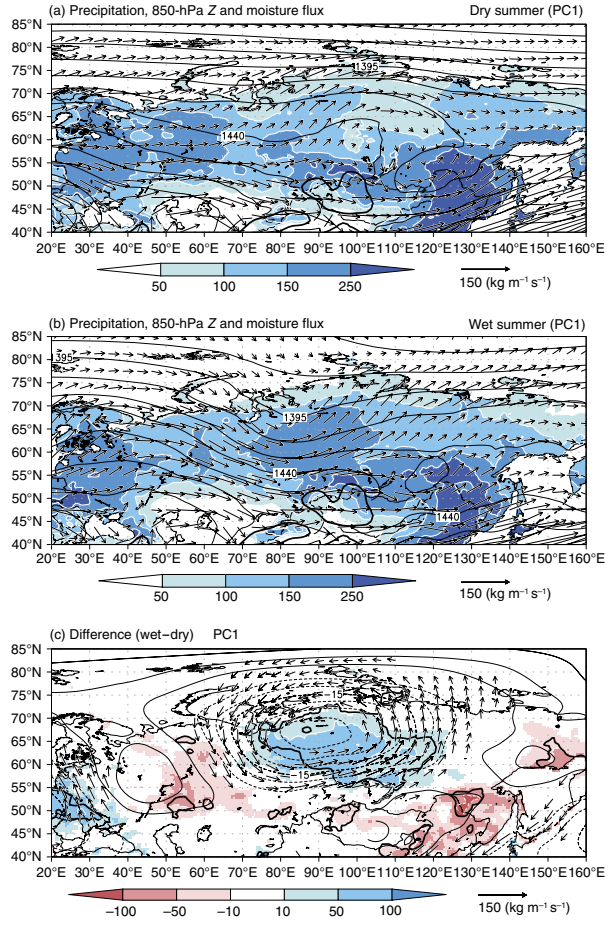

Figure 9. (a) Composite of 3-month total precipitation (shading, mm (3 months)$^{-1}$), the 850-hPa geopotential height (contours, interval 15 gpm), and vertically integrated moisture flux vectors for dry summers based on PC1. (b) As in (a) but for wet summers. (c) As in (a) but for the difference between wet and dry summers, and with a contour interval for geopotential height of 5 gpm. Only moisture flux vectors that are statistically significant difference at the 95% level are plotted. Shaded areas enclosed by thick solid lines indicate a significant difference at the 95% confidence level in precipitation.

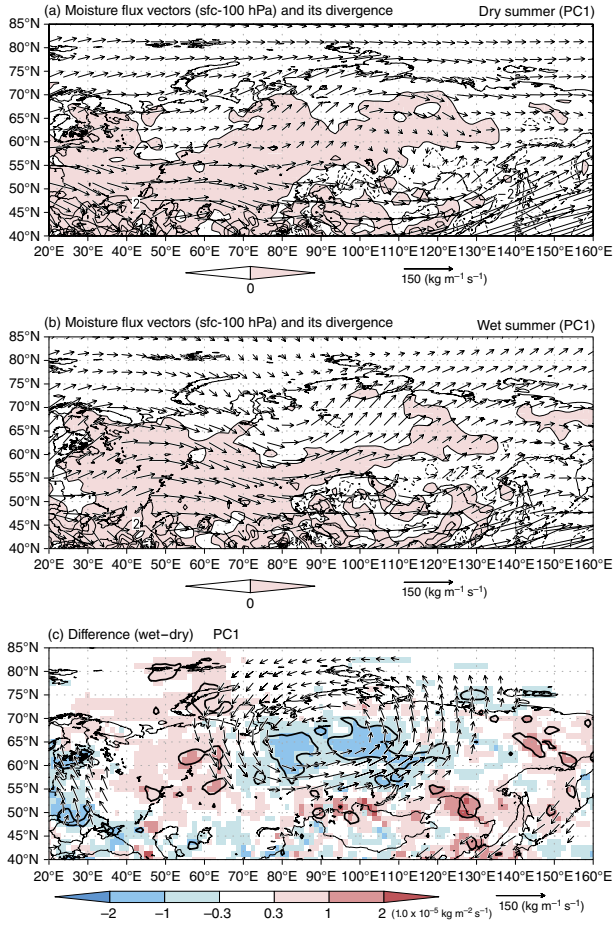

Figure 10. (a) Composite of vertically integrated moisture flux vectors and its divergence (contours, interval 2.0×10^{-5} kg m^{-2} s^{-1}) for dry summers based on PC1. Areas of divergence are shaded. (b) As in (a) but for wet summers. (c) As in (a) but for the difference between wet and dry summers. Only moisture flux vectors that are statistically significant difference at the 95% level are plotted. Shaded areas enclosed by thick solid lines indicate a significant difference at the 95% confidence level in moisture flux divergence. The unit for moisture flux divergence is 1.0×10^{-5} kg m^{-2} s^{-1}.

robust large-scale atmospheric circulation signals are discernible in the two modes from the regression analysis.

Figure 9 shows composites of precipitation, Z850, and the integrated moisture flux vectors for dry and wet summers in EOF1. We selected the six driest summers (1984, 1990, 1992, 1994, 2003, and 2006) and the six wettest summers (1980, 1988, 1991, 1997, 2001, and 2007) for each composite, based on the PC1 time series. Figure 10 is the same as Figure 9, but for the moisture flux vectors and divergence. In a dry summer, an anti-cyclonic circulation dominates over eastern Siberia, with the ridge-line along 105°E (Figure 9(a)). The divergence area of the moisture flux vectors extends widely over eastern Siberia under the anti-cyclonic circulation (Figure 10(a)). In contrast, in a wet summer, the ridge disappears over eastern Siberia (Figure 9(b)), replaced by a cyclonic circulation with a trough line along 80°E that influences eastern Siberia. Strong southwesterly/westerly moisture fluxes dominate over eastern Siberia. Areas of moisture convergence expand over eastern Siberia, especially around the central Siberian Plateau where precipitation shows a large increase (Figure 9(b)). The composite difference reveals a similar spatial structure to the regression pattern in Figure 8(a) (Figure 9(c)). The positive precipitation anomaly over eastern Siberia is associated with a low-level cyclonic circulation anomaly centred at around 65°N, 90°E. The positions of the positive and negative rainfall anomalies correspond to convergent and divergent anomalies of the moisture flux, respectively (Figures 9(c) and 10(c)).

Based on PC2, we selected the six driest (1985, 1986, 1991, 1998, 2001, and 2002) and six wettest (1981, 1982, 1994, 2005, 2006, and 2007) summers for the EOF2 mode. Note that the wet and dry years for the EOF2 mode represent high and low precipitation years in the eastern part of eastern Siberia (i.e. the Lena river basin), respectively. Dry summers in EOF2 are characterised by a deep trough along 80°E over the West Siberian Plain (Figure 11(a)). In contrast, in a wet summer, westerly moisture flux vectors are observed from the West

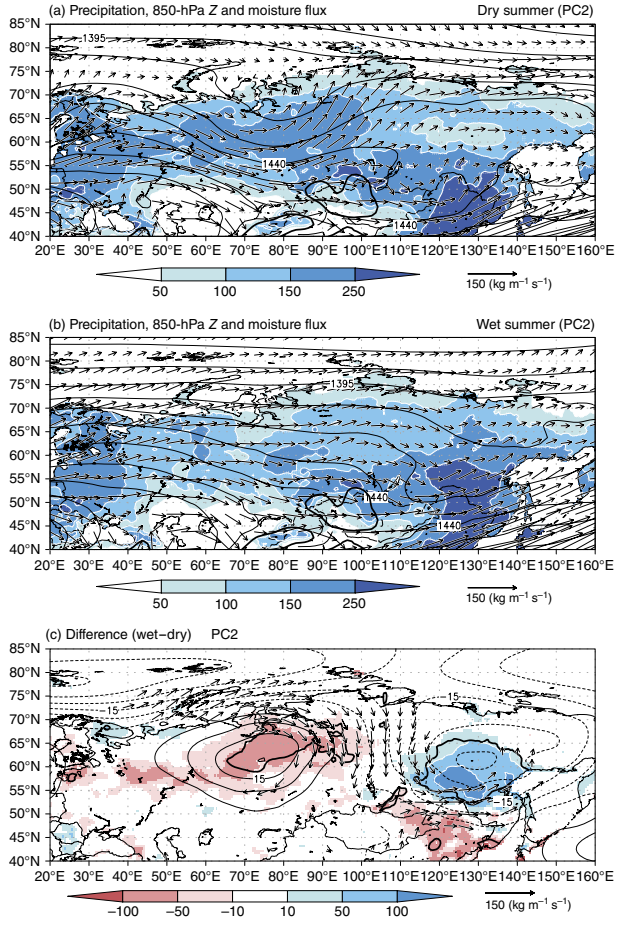

Figure 11. (a) Composite of 3-month total precipitation (shading, mm (3 months)$^{-1}$), the 850-hPa geopotential height (contours, interval 15 gpm), and vertically integrated moisture flux vectors for dry summers based on PC2. (b) As in (a) but for wet summers. (c) As in (a) but for the difference between wet and dry summers, and with a contour interval for geopotential height of 5 gpm. Only moisture flux vectors that are statistically significant difference at the 95% level are plotted. Shaded areas enclosed by thick solid lines indicate a significant difference at the 95% confidence level in precipitation.

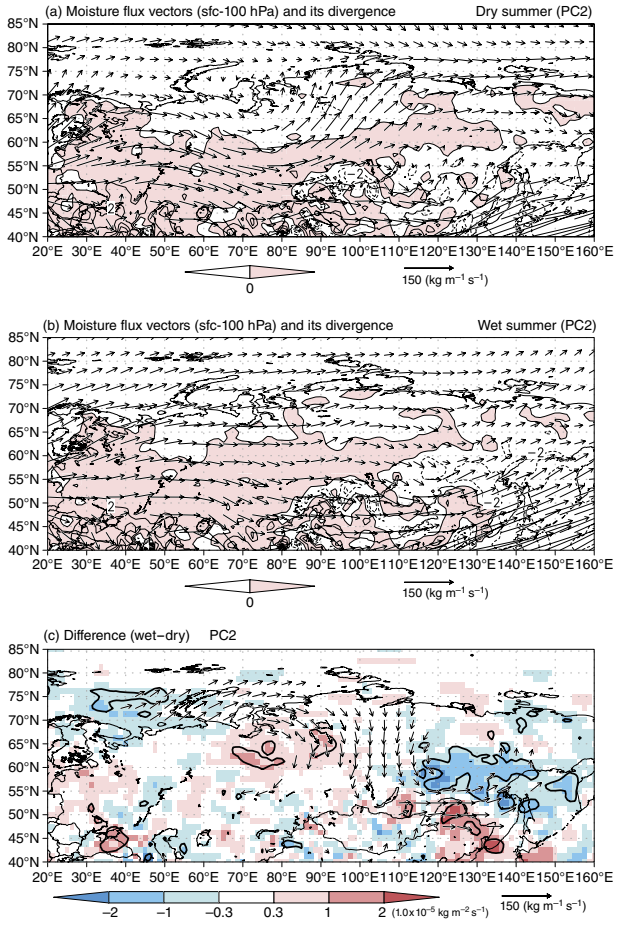

Figure 12. (a) Composite of vertically integrated moisture flux vectors and its divergence (contours, interval 2.0×10^{-5} kg m^{-2} s^{-1}) for dry summers based on PC2. Areas of divergence are shaded. (b) As in (a) but for wet summers. (c) As in (a) but for the difference between wet and dry summers. Only moisture flux vectors that are statistically significant difference at the 95% level are plotted. Shaded areas enclosed by thick solid lines indicate a significant difference at the 95% confidence level in moisture flux divergence. The unit for moisture flux divergence is 1.0×10^{-5} kg m^{-2} s^{-1}.

Siberian Plain to the western part of eastern Siberia, where the deep trough lies in dry summers, with no distinct cyclonic or anti-cyclonic circulation. Of note, a deep trough extends from 55°N, 115°E to 65°N, 140°E over the upper/middle reaches of the Lena river basin (Figure 11(b)). Westerly/southwesterly moisture fluxes are enhanced and converge over the southeastern side of the trough (Figure 12(b)). The trough results in enhanced westerly moisture flow over Siberia, and the southwesterly moisture flux from the Asian monsoon region south of 50°N seems to converge over the easternmost part of eastern Siberia. The composite difference shows an east–west dipole of circulation anomalies between the Obi and Lena river basins (Figure 11(c)), similar to the regression pattern in Figure 8(b). The difference in summer precipitation is more than 100 mm around the middle reaches of the Lena river basin (Figure 11(c)). The distribution of precipitation anomalies corresponds to the distribution of moisture flux divergence between the two basins (Figure 12(c)), suggesting that the difference in precipitation is induced by changes in the atmospheric circulation and the associated moisture flux divergence.

The precipitation anomalies in the eastern Siberia domain (Figures 9(c) and 11(c)) are accompanied by changes in precipitation characteristics, including frequency and intensity. Climatologically, both the frequency and intensity of precipitation are high in the southern part of the domain (Figure 13(a) and (e)). A large increasing trend in frequency occurs over and around the Central Siberian Plateau and the northern part of eastern Siberia (Figure 13(b)), resulting in the increasing trend in summer precipitation seen in Figure 4. In contrast, the decreasing precipitation around the lower reaches of the Amur river basin is attributed to a decrease in both precipitation frequency and intensity. In EOF1, the area of the positive precipitation anomaly around the Central Siberian Plateau corresponds to the area with high precipitation frequency (Figures 9(c) and 13(c)). The spatial pattern of the precipitation frequency is also similar to that of EOF1 (Figure 7(a)). Of note, there is no marked change in

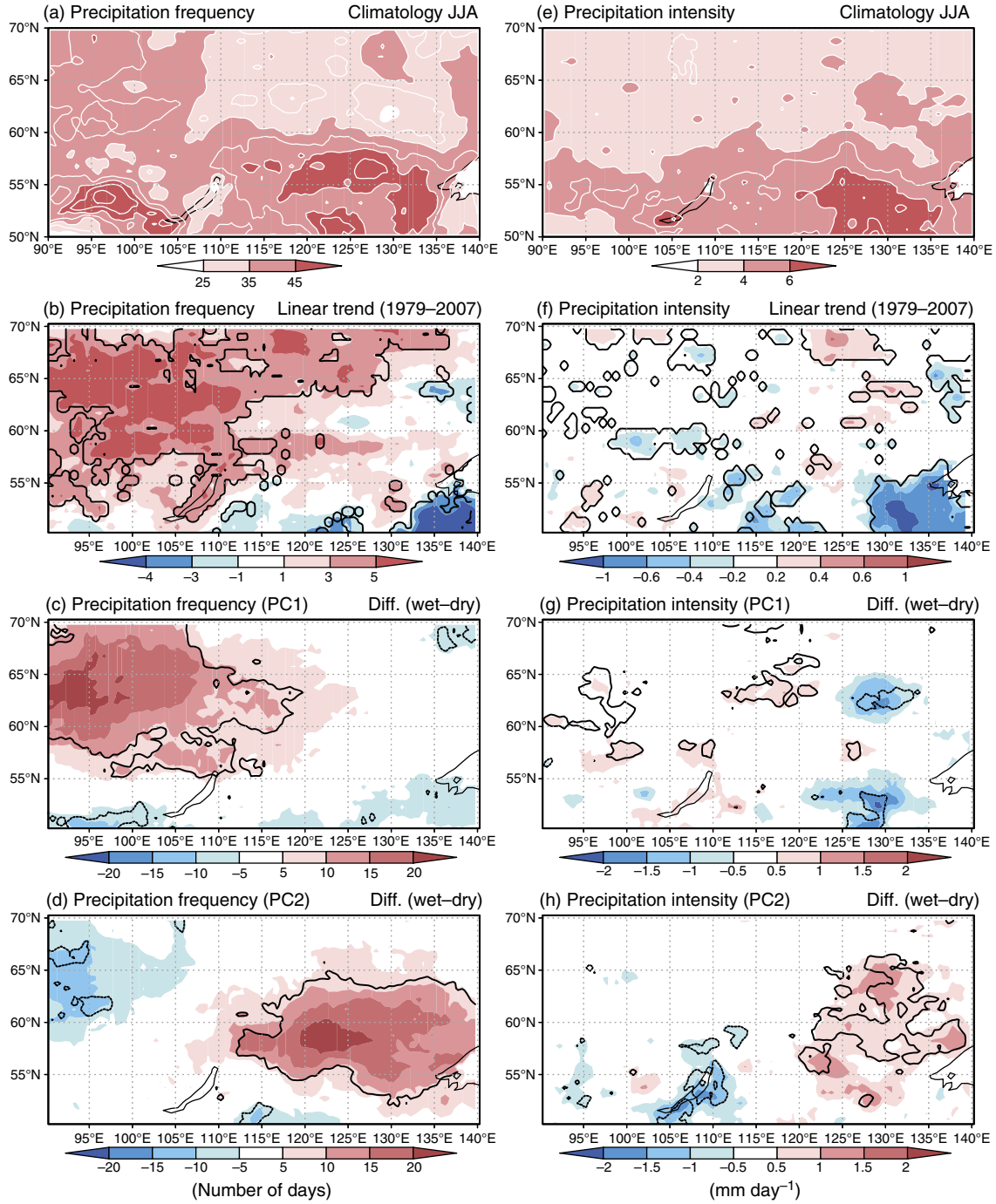

Figure 13. (a) Climatological mean (1979–2007) precipitation frequency in summer (JJA), defined as the average number of days per JJA period with precipitation exceeding 1 mm day^{-1}. The contour interval is five days. (b) Linear trend (per decade) of precipitation frequency for 1979–2007. Shaded areas enclosed by thick solid lines indicate significance at the 95% level (Mann-Kendall test). (c) Difference in the frequency of precipitation during JJA between wet and dry summers based on PC1. Shaded areas enclosed by a thick solid line indicate a significant difference at the 95% confidence level. (d) As in (c), but for PC2. (e)-(h) As in (a)-(d), but for precipitation intensity. The contour interval for (e) is 1 mm day^{-1}. The unit is mm day^{-1} in (f), (g) and (h).

precipitation intensity (Figure 13(g)). The spatial pattern of precipitation frequency for EOF2 resembles that of the precipitation itself (Figures 13(d) and 7(b)), indicating that the change in the distribution of precipitation is caused by a change in precipitation frequency. Additionally, the increase in precipitation intensity also contributed to the higher precipitation around the middle reaches of the Lena river basin (Figure 13(h)).

The patterns of atmospheric structure in both the EOF1 and EOF2 modes are related to the changes in quasi-stationary wave patterns (i.e. troughs and ridges) across northern Eurasia along the Arctic frontal zone. In EOF1, the wave train structure is observed in both the lower and upper troposphere across Siberia from western Europe to east of the Verkhoyansk Mountains, where the jet exit region of the North Atlantic and the polar jet

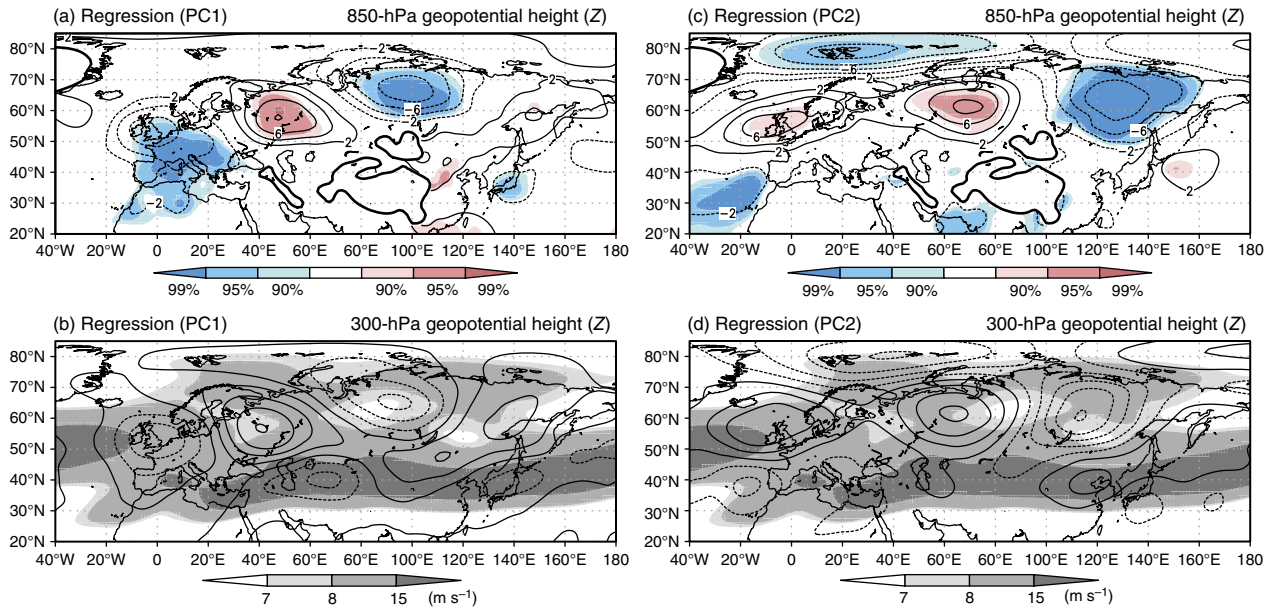

Figure 14. Regression patterns of geopotential height at (a) 850 hPa and (b) 300 hPa against PC1. (a) The contour interval is 2 gpm and the zero contour is omitted. The colour shading represents the confidence level of the correlation coefficient between PC1 and the geopotential height at 850 hPa. The topographic contour for 1500 m is shown as a thick solid line. (b) The contour interval is 6 gpm, and the contours start from ±3 gpm. The zero contour is omitted. Shading denotes areas of zonal wind speed greater than 7 m s^{-1}. (c) and (d) As in (a) and (b), but for PC2.

are located (Figure 14(a) and (b)). The cyclonic circulation related to wet summers in eastern Siberia is part of this wave train. The vertical structure of geopotential anomalies is barotropic in the upstream area over England. However, it appears to change into a more vertically baroclinic structure over eastern Siberia. Another wave pattern is also found along the Asian subtropical jet south of the northern wave train along the polar jet (Figure 14(b)). The anomaly pattern seen in Figure 14(b) is similar to that presented by Iwao and Takahashi (2006), who interpreted it as the eastward energy dispersion of a quasi-stationary Rossby wave along the Arctic polar and Asian jets. In EOF2, the wave pattern tends to be confined along the jet exit region of the Atlantic Ocean and the Arctic polar jet (Figure 14(c) and (d)). Generally, the vertical structure of the wave is barotropic except in eastern Siberia where the vertical structure tilts westward. Note that there are two significant geopotential anomalies: over the jet exit region in the Northern Atlantic and the entrance region of the polar jet to the north of the Scandinavian Peninsula. This is indicative of a dynamic link in the fluctuation between the east–west dipole over Siberia and the two upstream anomalies.

4. Discussion

4.1. Increasing trend in summer precipitation over eastern Siberia

The increasing trend in summer precipitation is remarkable over eastern Siberia (Figure 4). The raw precipitation time series over eastern Siberia shows a large interannual variability superimposed on the long-term trend (Figure 5). The trend in atmospheric circulation at 850 hPa is marked by decreasing geopotential height over and around Siberia, and increasing geopotential height around Mongolia and western Russia (Figure 6). The spatial variation of trends in geopotential height over and around Siberia suggests that atmospheric circulation changes contribute to the increasing trend in precipitation over eastern Siberia (Figure 6). The circulation changes indeed enhance eastward moisture transport and its convergence over eastern Siberia (Figures 5 and 6). Thus, moisture flux divergence is probably a key factor that causes variability in precipitation over eastern Siberia.

APHRODITE and the other monthly precipitation datasets use the data available through the GTS network. The APHRODITE-RU dataset also includes individual data correction additional to that used for the GTS gauge network (Yatagai *et al.*, 2012). Rain gauges often measure rainfall with large errors, especially for solid precipitation (i.e. snowfall), and wind-induced negative biases for snowfall measurements are higher than for other precipitation types. Warming around Siberia might cause an artificial increase in the measured precipitation in winter (Groisman *et al.*, 2014). In summer, the trend in surface temperature around the region with a significant increasing trend of summer precipitation does not show any clear warming during 1979–2012 (Ding *et al.*, 2014; their extended data Figure 2(c)). This suggests that where solid precipitation falls in summer, any artificial increase related to warming due to reduced wind-induced negative biases for solid precipitation is small over eastern Siberia. Instead, the circulation changes can explain the increasing trend in precipitation: moisture flux convergence has been increasing there in recent decades. However, we still need to examine the effects of systematic bias of gauge

measurements in order to assess the precipitation trend more quantitatively.

The regression pattern of Z850 based on PC1 shows that the interannual variations are associated with the quasi-stationary trough centred around the Central Siberian Plateau (Figure 8(a)). The regression pattern is similar to the trend pattern of Z850 around Siberia (Figures 6 and 8(a)). This means that a combination of the trend and EOF1 are responsible for the raw precipitation time series seen in Figure 5. It also suggests that a deeper quasi-stationary trough has probably appeared with growing frequency around eastern Siberia in recent decades. It is important to determine the precipitation systems that generate the increase in precipitation under this quasi-stationary trough, for which cyclones are a possible candidate. The east–west seesaw oscillation in precipitation and wave pattern, which corresponds to EOF2 (Figures 8(b) and 11(c)), is clearly related to the east–west shifting of storm tracks across Siberia (Fukutomi *et al.*, 2007). The decreasing trend of Z850 and the interannual variation of circulation anomalies over eastern Siberia might indicate a change in cyclone tracks and frequency in recent decades. Further study is required to fully resolve this issue.

4.2. Large-scale atmospheric circulation related to precipitation variability in eastern Siberia

It is clear that the quasi-stationary troughs related to EOF1 and EOF2 are part of the wave-train-like structures along the polar jet, and this is indicative of a dynamic linkage between the windward regions through Rossby wave dispersion. The polar jet acts as a waveguide for the Rossby wave, as does the Asian subtropical jet (Ding and Wang, 2005). Both wave trains can be traced back to the Atlantic Ocean region. However, the wave sources of these wave trains remain unclear. It has been reported that the recent decline in sea-ice extent in the Arctic Ocean may change atmospheric circulation patterns (Screen, 2013; Cassano *et al.*, 2014). Alternatively, a Rossby wave train originating from the tropics, driven by sea surface temperature (SST) forcing, may affect the Arctic region (Ding *et al.*, 2014). The variation in summer monsoon rainfall over South Asia could also affect the recent rapid ice melt over the Arctic Ocean through a teleconnecion (Krishnamurti *et al.*, 2015). Further studies are required to determine the sources of the atmospheric circulation changes around eastern Siberia, related to both the interannual variation and the long-term trend.

A continued decline in summer sea ice cover has been observed in the Arctic (Ogi and Wallace, 2007; Comiso *et al.*, 2008) and may be an important factor in climate change in the region. Of note, a remarkable decline has been observed over marginal seas such as the Kara Sea and Laptev Sea north of eastern Siberia. Figure 15 shows the regression patterns of the geopotential height at 925 hPa against the time series of normalised raw precipitation from APHRODITE-RU over eastern Siberia (Figure 5) for the circum-Arctic region. The regression pattern in

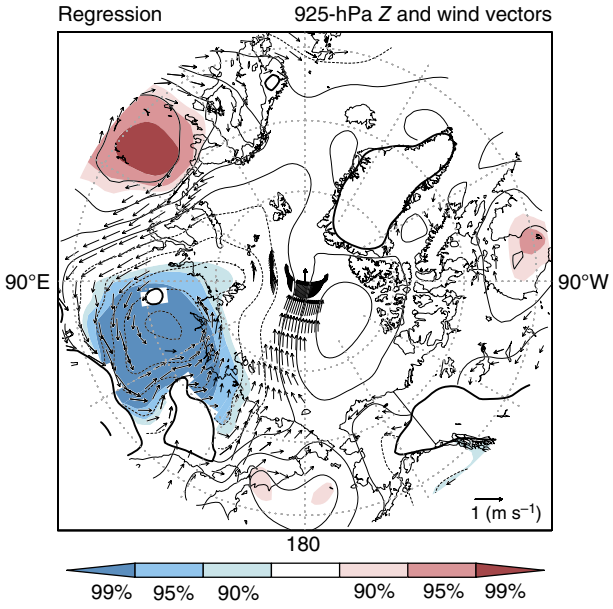

Figure 15. Regression pattern of geopotential height and wind vectors at 925 hPa based on normalised area-averaged (55°–70°N, 90–130°E) time series of precipitation. The colour shading represents the confidence level of the correlation coefficient between the time series and the geopotential height at 925 hPa. Blue (red) shading indicates negative (positive) correlation. The contour interval for geopotential height is 2 gpm. Only wind vectors that are statistically significant at the 90% level are plotted. The topographic contour for 750 m is shown as a thick solid line.

Figure 15 resembles that of sea level pressure against the time series of the extent of September Arctic sea ice, which has declined substantially since 1979, especially north of eastern Siberia and Alaska (Figure 4(a) of Ogi and Wallace, 2007). The pattern is characterised by a cyclonic circulation anomaly around eastern Siberia and an anti-cyclonic anomaly over the Arctic Ocean. The atmospheric circulation anomaly can induce an easterly wind anomaly that could reduce Arctic sea ice cover (Ogi and Wallace, 2007; Ogi *et al.*, 2008). Thus, the increasing trend and interannual variation in summer precipitation over eastern Siberia, and the related atmospheric circulation, may have a dynamic connection with the recent decline in Arctic ice during late summer.

4.3. Recent wet years in eastern Siberia and their impact on the hydroclimate

Recent *in situ* observations at Spasskaya Pad (62.2°N, 129.1°E) near Yakutsk, eastern Siberia, where the action centre of precipitation in EOF2 is located (Figure 7(b)), indicate that wet years occurred from 2005 to 2008 and dry years from 2001 to 2004 (Hiyama *et al.*, 2013; Ohta *et al.*, 2014), consistent with the features of the PC2 time series (Figure 7(e)). Successive wet years from 2005 to 2008 damaged the taiga forest due to water logging and changed the characteristics of the hydroclimate. Soil moisture, soil temperature, and annual maximum thawing depth increased after the wet year of 2005 (Hiyama *et al.*, 2013; Ohta *et al.*, 2014). The taiga–permafrost ecosystem is unique to eastern Siberia and is maintained under

a low-precipitation climate. The 2005–2008 wet summers around Yakutsk were induced by the wet phase of EOF2 that fluctuates on a 6–8-year period. The weak increasing trend may also affect the middle reaches of the Lena river basin at longitudes of 110°–130°E (Figure 4). Thus, from 2005 to 2007 the Lena river basin as a whole received high rainfall, probably due to a combination of the long-term trend and the EOF2 mode. Because precipitation is an important parameter maintaining the taiga–permafrost ecosystem, increased precipitation may change the features of the hydroclimate and the ecosystem in the future. Thus, monitoring the hydroclimate over eastern Siberia, and determining how the ecosystem reacts to increasing precipitation, is important for the understanding of water and carbon cycles in this region.

5. Conclusions

The forest–permafrost coupled ecosystem of eastern Siberia is maintained under conditions of low precipitation and is sensitive to changes in precipitation. Using daily gridded precipitation datasets for the period from 1979 to 2007, we investigated the long-term trend and leading modes of interannual variation in summer precipitation over eastern Siberia in recent decades. Atmospheric circulation patterns related to the trend and the first three leading modes were also examined using an atmospheric reanalysis dataset. The results are summarised as follows.

1. We examined the long-term trend in summer (JJA) precipitation over eastern Siberia on a seasonal total basis. A significant increasing trend in summer precipitation is observed over eastern Siberia (e.g. the Yenisei and Lena river basins). The time series of area-averaged summer total precipitation for 55°–70°N, 90°–130°E shows a linear trend with a 13.9-mm increase per decade over 1979–2007, which is significant at the 99% level (Mann–Kendall test). Summer mean 850-hPa geopotential height decreases from Siberia to the marginal seas north of Siberia, with the largest decreases occurring over the northern part of eastern Siberia, while significant increases are found around Mongolia. The trend in geopotential height induces a significant increase in westerly moisture flux vectors and their convergence over eastern Siberia, probably resulting in the rainfall increase over eastern Siberia.
2. To examine the dominant spatiotemporal patterns of summer precipitation variability, EOF analysis was applied to normalised and detrended JJA precipitation over the east Siberian domain (50°–70°N, 90°–140°E) for the period 1979–2007. The first leading mode (EOF1) represents interannual variation with a 3–5-year period centred over the Central Siberian Plateau, including the middle reaches of the Yenisei river basin and a large area of the Lena river basin, from the upper to lower reaches. This mode accounts for 20.2% of the total variance. The spatial pattern of EOF1 is similar to the trend pattern. The second leading mode (EOF2; 17.5%) shows a dipole pattern between the middle reaches of the Lena river basin centred around 130°E, 60°N and the western part of the central Siberian Plateau, with a large interannual variation with a period of 6–8 years. In the third mode (EOF3; 11.9%), the pattern represents the variation between the northeastern mountainous region (the Verkhoyansk Mountains), the region around the border with Mongolia, and the latitudes from 55° to 65°N. However, the values of EOF3 are small over the entire domain compared with those seen in EOF1 and EOF2.
3. Robust large-scale atmospheric circulation signals are discernible in relation to the first two leading modes, while relatively local and weak circulation signals are associated with the third mode. Regression analysis of the geopotential height at 850 hPa based on PC1 shows that high summer precipitation is related to a cyclonic circulation anomaly centred at around 65°N, 100°E that extends over an area from eastern Siberia to the Arctic seas around Siberia. The regression pattern is similar to the spatial pattern of the long-term trend in geopotential height. A deeper quasi-stationary trough appears with increasing frequency in recent decades, superimposed on the long-term trend. The regression pattern for EOF2 shows a dipole pattern between the Obi and Lena river basins. The high summer precipitation around the upper and middle reaches of the Lena river basin is related to the low-level cyclonic circulation anomaly centred around 60°N, 130°E. Weak and relatively local cyclonic anomalies surround the positive values seen in EOF3.
4. The circulation patterns of the first two leading modes are related to changes in the stationary trough and ridge systems along the Arctic polar jet. The composite of geopotential height at 850 hPa in the wet summers identified using PC1 shows that a large-scale stationary trough appears with its axis along 80°E over Siberia, and this trough influences eastern Siberia. Southwesterly/westerly moisture flux vectors are in turn enhanced over the whole of eastern Siberia. The areas of moisture convergence then expand over eastern Siberia. The EOF2 composite of wet summers shows that a stationary trough is observed around 120°–130°E over the upper/middle reaches of the Lena river basin. The westerly/southwesterly moisture fluxes are enhanced and converge east of the trough, producing high rainfall.
5. The regression pattern in geopotential height based on PC1 shows a wave train structure from the exit region of the North Atlantic jet over Western Europe, across Siberia to the east of the Verkhoyansk Mountains where the exit region of the Arctic polar jet is located. The cyclonic circulation related to wet summers of the EOF1 mode in eastern Siberia is part of this wave train. Another wave pattern is also found along the Asian subtropical jet south of the northern wave train. In EOF2, the wave pattern tends to be confined to the exit region of the Atlantic Ocean and the Arctic

polar jet. There are significant geopotential anomalies over the jet exit region in the Northern Atlantic and the jet entrance region of the polar jet to the north of the Scandinavian Peninsula, indicating a dynamic link in the fluctuation between the east–west dipole over Siberia and the two upstream anomalies.

Acknowledgements

We thank Prof. Tetsuya Hiyama of Nagoya University for his many valuable comments. We also thank Dr Rikie Suzuki of the Department of Environmental Geochemical Cycle Research at JAMSTEC for providing the NDVI datasets, Dr Kanamori for helpful comments and support with data processing, and Dr Yatagai of Nagoya University and Dr Arakawa of Tsukuba University for making valuable comments on the details of the APHRODITE dataset. The APHRODITE-RU V1101 dataset was obtained from the project web site (http://www.chikyu.ac.jp/precip/). This study was partly supported by Research Project No. C-07 of the Research Institute for Humanity and Nature (RIHN), entitled 'Global Warming and the Human-Nature Dimension in Siberia: Social Adaptation to the Changes of the Terrestrial Ecosystem, with an Emphasis on Water Environments'(PI: T. Hiyama). Portions of this study were conducted as part of a collaborative research program of the Hydrospheric Atmospheric Research Center, Nagoya University.

References

Cassano EN, Cassano JJ, Higgins ME, Serreze MC. 2014. Atmospheric impacts of an Arctic sea ice minimum as seen in the Community Atmosphere Model. *Int. J. Climatol.* **34**: 766–779, doi: 10.1002/joc.3723.

Chen MY, Xie PP, Janowiak JE, Arkin PA. 2002. Global land precipitation: a 50-yr monthly analysis based on gauge observations. *J. Hydrometeorol.* **3**: 249–266, doi: 10.1175/1525-7541(2002)003<0249:GLPAYM>2.0.CO;2.

Comiso JC, Parkinson CL, Gersten R, Stock L. 2008. Accelerated decline in the Arctic sea ice cover. *Geophys. Res. Lett.* **35**: L01703, doi: 10.1029/2007GL031972.

Ding Q, Wang B. 2005. Circumglobal teleconnection in the Northern Hemisphere summer. *J. Clim.* **18**: 3483–3505, doi: 10.1175/JCLI3473.1.

Ding Q, Wallace JM, Battisti DS, Steig EJ, Gallant AJE, Kim HJ, Geng L. 2014. Tropical forcing of the recent rapid Arctic warming in northeastern Canada and Greenland. *Nature* **509**: 209–212, doi: 10.1038/nature13260.

Fukutomi Y, Igarashi H, Masuda K, Yasunari T. 2003. Interannual variability of summer water balance components in three major river basins of Northern Eurasia. *J. Hydrometeorol.* **4**: 283–296, doi: 10.1175/1525-7541(2003)4<283:IVOSWB>2.0.CO;2.

Fukutomi Y, Masuda K, Yasunari T. 2004. Role of storm track activity in the interannual seesaw of summer precipitation over northern Eurasia. *J. Geophys. Res. Atmos.* **109**: D02109, doi: 10.1029/2003JD003912.

Fukutomi Y, Masuda K, Yasunar T. 2007. Cyclone activity associated with the interannual seesaw oscillation of summer precipitation over northern Eurasia. *Glob. Planet. Change* **56**: 387–398, doi: 10.1016/j.gloplacha.2006.07.026.

Groisman PY, Bogdanova EG, Alexeev VA, Cherry JE, Bulygina ON. 2014. Impact of snowfall measurement deficiencies on quantification of precipitation and its trends over northern Eurasia. *Ice Snow* **126**: 29–43 (in Russian with English abstract).

Hiyama T, Ohta T, Sugimoto A, Yamazaki T, Oshima K, Yonenobu H, Yamamoto K, Kotani A, Park H, Kodama Y, Hatta S, Fedorov AN, Maximov TC. 2013. Changes in eco-hydrological system under recent climate change in eastern Siberia. In *Cold and Mountain Region Hydrological Systems Under Climate Change: Towards Improved Projections* Proceedings of H02, IAHS Publication No. 360, IAHS-IAPSO-IASPEI Assembly, Gothenburg, Sweden, July 2013, 155–160.

Iwao K, Takahashi M. 2006. Interannual change in summertime precipitation over northeast Asia. *Geophys. Res. Lett.* **33**: L16703, doi: 10.1029/2006GL027119.

Krishnamurti TN, Krishnamurti R, Das S, Kumar V, Jayakumar A, Simon A. 2015. A pathway connecting the monsoonal heating to the rapid Arctic ice melt. *J. Atmos. Sci.* **72**: 5–34, doi: 10.1175/JAS-D-14-0004.1.

Kurita N, Yoshida N, Inoue G, Chayanova EA. 2004. Modern isotope climatology of Russia: a first assessment. *J. Geophys. Res. Atmos.* **109**: D03102, doi: 10.1029/2003JD003404.

Ogi M, Wallace JM. 2007. Summer minimum Arctic sea ice extent and the associated summer atmospheric circulation. *Geophys. Res. Lett.* **34**: L12705, doi: 10.1029/2007GL029897.

Ogi M, Rigor IG, McPhee MG, Wallace JM. 2008. Summer retreat of Arctic sea ice: role of summer winds. *Geophys. Res. Lett.* **35**: L24701, doi: 10.1029/2008GL035672.

Ohta T, Hiyama T, Tanaka H, Kuwada T, Maximov TC, Ohata T, Fukushima Y. 2001. Seasonal variation in the energy and water exchanges above and below a larch forest in eastern Siberia. *Hydrol. Processes* **15**: 1459–1476, doi: 10.1002/hyp.219.

Ohta T, Maximov TC, Dolman AJ, Nakai T, van der Molen MK, Kononov AV, Maximov AP, Hiyama T, Iijima Y, Moors EJ, Tanaka H, Toba T, Yabuki H. 2008. Interannual variation of water balance and summer evapotranspiration in an eastern Siberian larch forest over a 7-year period (1998–2006). *Agric. For. Meteorol.* **148**: 1941–1953, doi: 10.1016/j.agrformet.2008.04.012.

Ohta T, Kotani A, Iijima Y, Maximov TC, Ito S, Hanamura M, Kononov AV, Maximov AP. 2014. Effects of waterlogging on water and carbon dioxide fluxes and environmental variables in a Siberian larch forest, 1998–2011. *Agric. For. Meteorol.* **188**: 64–75, doi: 10.1016/j.agrformet.2013.12.012.

Onogi K, Tsutsui J, Koide H, Sakamoto M, Kobayashi S, Hatsushika H, Matsumoto T, Yamazaki N, Kamahori H, Takahashi K, Kadokura S, Wada K, Kato K, Oyama R, Ose T, Mannoji N, Taira R. 2007. The JRA-25 reanalysis. *J. Meteorol. Soc. Jpn.* **85**: 369–432, doi: 10.2151/jmsj.85.369.

Osawa A, Zyryanova OA, Matsuura Y, Kajimoto T, Wein RW (eds). 2010. *Permafrost Ecosystems: Siberian Larch Forests*. Springer: New York, NY, 502 pp.

Saito K, Yasunari T, Takata K. 2006. Relative roles of large-scale orography and land surface processes in the global hydroclimate. Part II: impacts on hydroclimate over Eurasia. *J. Hydrometeorol.* **7**: 642–659, doi: 10.1175/JHM516.1.

Schneider U, Becker A, Finger P, Meyer-Christoffer A, Ziese M, Rudolf B. 2014. GPCC's new land surface precipitation climatology based on quality-controlled in situ data and its role in quantifying the global water cycle. *Theor. Appl. Climatol.* **115**: 15–40, doi: 10.1007/s00704-013-0860-x.

Screen JA. 2013. Influence of Arctic sea ice on European summer precipitation. *Environ. Res. Lett.* **8**: 044015, doi: 10.1088/1748-9326/8/4/044015.

Serreze MC, Etringer AJ. 2003. Precipitation characteristics of the Eurasian Arctic drainage system. *Int. J. Climatol.* **23**: 1267–1291, doi: 10.1002/joc.941.

Serreze MC, Bromwich DH, Clark MP, Etringer AJ, Zhang TJ, Lammers R. 2003. Large-scale hydro-climatology of the terrestrial Arctic drainage system. *J. Geophys. Res. Atmos.* **107**(D2): 8160, doi: 10.1029/2001JD000919.

Smith PM, Kalluri SNV, Prince SD, DeFries R. 1997. The NOAA/NASA pathfinder AVHRR 8-km land dataset. *Photogramm. Eng. Remote Sens.* **63**: 12–31.

Sugimoto A, Yanagisawa N, Naito D, Fujita N, Maximov TC. 2002. Importance of permafrost as a source of water for plants in east Siberian taiga. *Ecol. Res.* **17**: 493–503, doi: 10.1046/j.1440-1703.2002.00506.x.

Suzuki R, Masuda K, Dye DG. 2007. Interannual covariability between actual evapotranspiration and PAL and GIMMS NDVIs of northern Asia. *Remote Sens. Environ.* **106**: 387–398, doi: 10.1016/j.rse.2006.10.016.

Wilks DN. 2011. Chapter 12: Principal component (EOF) analysis. In *Statistical Methods in the Atmospheric Sciences*, 3rd edn. Academic Press, Oxford, UK, 519–562.

Willmott CJ, Matsuura K. 1995. Smart interpolation of annually averaged air temperature in the United States. *J. Appl. Meteorol.* **34**: 2577–2586, doi: 10.1175/1520-0450(1995)034<2577:SIOAAA>2.0.CO;2.

Yatagai A. 2003. Evaluation of hydrological balance and its variability in arid and semi-arid regions of Eurasia from ECMWF 15 year reanalysis. *Hydrol. Processes* **17**: 2871–2884, doi: 10.1002/Hyp.1439.

Yatagai A, Kamiguchi K, Arakawa O, Hamada A, Yasutomi N, Kitoh A. 2012. APHRODITE: constructing a long-term daily gridded precipitation dataset for Asia based on a dense network of rain gauges. *Bull. Am. Meteorol. Soc.* **93**: 1401–1415, doi: 10.1175/BAMS-D-11-00122.1.

Yoshida R, Sawada M, Yamazaki T. 2011. Roles of eastern Siberian mountain ranges in precipitation – Verkhoyansk, Dzhugdzhur and Stanovoy mountain ranges. *SOLA* **7**: 145–148, doi: 10.2151/sola.2011-037.

Zhang N, Yasunari T, Ohta T. 2011. Dynamics of the larch taiga–permafrost coupled system in Siberia under climate change. *Environ. Res. Lett.* **6**: 024003, doi: 10.1088/1748-9326/6/2/024003.

